

Article

# Shellac Thin Films Obtained by Matrix-Assisted Pulsed Laser Evaporation (MAPLE)

Simona Brajnicov <sup>1,2</sup>, Adrian Bercea <sup>1,3</sup>, Valentina Marascu <sup>1</sup>, Andreea Matei <sup>1,\*</sup> and Bogdana Mitu <sup>1</sup>

<sup>1</sup> National Institute for Lasers, Plasma, and Radiation Physics, 409 Atomistilor Street, P.O. Box MG-16, RO-077125 Magurele, Romania; brajnicov.simona@inflpr.ro (S.B.); bercea.adrian@inflpr.ro (A.B.); valentina.marascu@inflpr.ro (V.M.); mitub@infim.ro (B.M.)

<sup>2</sup> Faculty of Sciences, University of Craiova, RO-200585 Craiova, Romania

<sup>3</sup> CNRS, IRCER—UMR 7315, University of Limoges, F-87000 Limoges, France

\* Correspondence: andreea.matei@inflpr.ro

Received: 14 June 2018; Accepted: 3 August 2018; Published: 7 August 2018



**Abstract:** We report on the fabrication of shellac thin films on silicon substrates by matrix-assisted pulsed laser evaporation (MAPLE) using methanol as matrix. Very adherent, dense, and smooth films were obtained by MAPLE with optimized deposition parameters, such as laser wavelength and laser fluence. Films with a root mean square (RMS) roughness of 11 nm measured on  $40 \times 40 \mu\text{m}^2$  were obtained for a 2000-nm-thick shellac film deposited with  $0.6 \text{ J}/\text{cm}^2$  fluence at a laser wavelength of 266 nm. The MAPLE films were tested in simulated gastric fluid in order to assess their capabilities as an enteric coating. The chemical, morphological, and optical properties of shellac samples were investigated by Fourier transform infrared spectroscopy (FTIR), X-ray photoelectron spectroscopy (XPS), scanning electron microscopy (SEM), and atomic force microscopy (AFM).

**Keywords:** thin films; matrix-assisted pulsed laser evaporation; shellac; enteric coatings

## 1. Introduction

Shellac is a biomaterial, a resin secreted by the female lac bug *Kerria lacca* on the trees in India and Thailand. It consists of esters and polyesters of polyhydroxy acids. The main components of shellac are aleuritic and shellolic acid [1]. Other components can be butolic and jalaric acid [2]. The color can vary between light yellow and dark red depending on the origin of the raw material.

Shellac possesses very interesting properties, such as being UV resistant, and it is a barrier for water and a very good dielectric [3]. As a thin film, shellac can be easily deposited by drop casting from a solution with ethanol or methanol. Shellac thin films have a dielectric constant between 3 and 5 [3] and very low surface roughness. They have been used as a substrate for organic field-effect transistor (OFET) and as a gate dielectric [3]. When used as a substrate, a concentrated solution is prepared. The solution has to evaporate for about half an hour at  $50 \text{ }^\circ\text{C}$  and then it has to be heated for an hour at  $70 \text{ }^\circ\text{C}$  in order to obtain roughness lower than 1 nm [3].

Shellac is used in the food industry as a coating for fruits as protection against dehydration and for the glossy and attractive aspect [4]. Shellac can be added to the composition of food packaging materials for protection against bacteria and as a water repellent element [5]. Nail polish [6], furniture and wood varnish, and the protection of art objects [7] are some other applications shellac can be used for.

Shellac biopolymer can be used as a new carbon source for growing bubble-decorated graphene oxide films with high magneto-resistance as reported by Singhababu et al. in [8].

Improved properties for wood protection can be achieved for shellac films as a coating by dispersing inorganic nanoparticles (1–2%) in alcoholic shellac solution as demonstrated by

Weththimuni et al. in [9]. Increased hardness and increased UV resistance can be obtained using ZrO<sub>2</sub> and ZnO nanoparticles. The low cost and low processing temperature make shellac a good candidate for microfluidics applications via hot embossing in the same way standard polydimethylsiloxane (PDMS) is used [10].

In pharmaceuticals, shellac can be used for encapsulation and micro encapsulation [11] as an enteric coating due to its acidic character, delivering the drug to the colon for specific applications [12–14]. Kumpugdee-Vollrath et al. obtained controlled drug release using coatings of shellac and pectine in [15]. Coaxial electrospinning has been reported for the obtaining of shellac nanofibers for colon-targeted drug delivery by Wang et al. in [16].

In this work, we used a laser deposition technique to grow thin films of shellac for targeted drug release. The employed laser technique was Matrix-Assisted Pulsed Laser Evaporation (MAPLE), a variation of the pulsed laser deposition (PLD) procedure. Pulsed laser deposition is especially used in the deposition of inorganic thin films [17–19] and it cannot be used for all types of delicate materials. The PLD method can lead to their photochemical interaction when using laser emitting in UV. For polymers, organic materials, and materials with a complicated structure, the MAPLE system is preferred [20–22]. Important advantages arising from our approach using laser-based techniques are the good adherence, the high density of the films, and control over their thickness. Another important issue is the fact that MAPLE is a “dry technique”. During the coating procedure with MAPLE, the drug is not in contact with the matrix (solvent) and drug–solvent chemical interactions are therefore avoided.

MAPLE-grown films have been tested in simulated gastric fluid, where the resin coating offers the needed resistance to the stomach and small intestine environment [23].

## 2. Materials and Methods

Shellac wax-free was purchased from Sigma-Aldrich (St. Louis, MO, USA) and used as received. The MAPLE technique was employed using a low concentration of shellac (1–2 wt % dissolved in methanol). The solutions were poured into a copper target holder and they were frozen with liquid nitrogen. During the experiments, the targets were kept in a solid state. The influence of various laser wavelengths (266, 355, 532, and 1064 nm) on the deposition process was investigated. The laser fluence was in the range 0.6–2 J/cm<sup>2</sup> for the experiments using the UV wavelength and up to 4 J/cm<sup>2</sup> for the visible and IR wavelengths. We will present the results just for UV laser beam irradiation because green and infrared light did not lead to continuous films, most probably due to the fact that the methanol matrix does not absorb light at these wavelengths [24] and the target evaporation took place mainly on defects. The laser spot was set in the range 0.9–1 mm<sup>2</sup> for all the experiments. The substrates of 10 × 10 mm<sup>2</sup>, i.e., two side polished Si (100) wafer and quartz, were kept at room temperature and positioned at a distance of 4 cm from the target. The base pressure in the deposition chamber was ~8 × 10<sup>−6</sup> mbar and it increased during laser irradiation to 10<sup>−4</sup> mbar due to solvent evaporation. The number of pulses varied between 18,000 and 90,000 for a pulse repetition rate of 10 Hz. Before the deposition, the substrates were cleaned in an ultrasonic bath, using a standard procedure implying soap solution, water, acetone, and ethanol for 15 min each, and dried in a nitrogen gas flow.

For measuring the deposition rates of the films, contact profilometry studies were performed by means of a KLA-Tencor P-7 (Milpitas, CA, USA) step profiler equipped with a 2-μm radius and a 60° stylus working in contact with 2 mg applied force and scanning on a 3-mm length of the samples with a scan speed of 100 μm/s. Surface morphology was investigated by atomic force microscopy (AFM) and scanning electron microscopy (SEM) with an “XE-100” AFM produced by Park Systems (Suwon, South Korea) and a Quanta ESEM FEG 450 SEM (FEI, Hillsboro, OR, USA). Fourier transform infrared absorption spectra were acquired with a Jasco 6300 FTIR system (Oklahoma, OK, USA), in the range 4000–400 cm<sup>−1</sup>, with 4 cm<sup>−1</sup> resolution.

The wettability characteristics of the films were evaluated by contact angle measurements. The water contact angle was measured using an optical microscope KSV CAM101 (KSV Instruments

Ltd., Helsinki, Finland) with water drops of 0.5–1  $\mu\text{L}$  and by mediating the processed angles obtained upon five drops for each sample.

The simulated gastric fluid (SGF) dissolution media that is described in United States Pharmacopeia 33-28NF (2010) and European Pharmacopeia 7.0 (2010) was prepared as follows: 2.0 g NaCl, 3.2 g pepsin, 7.0 mL HCl, and 1000 mL milli q water. The solution used had a pH of 1.2. Shellac films deposited by MAPLE were immersed in SGF for 15, 30, 60, 120, and 240 min.

X-ray photoelectron spectroscopy (XPS) survey spectra and high-resolution XPS scan spectra were acquired for shellac dropcast, the initial film, and films immersed in SGF for different time durations using an Escalab Xi<sup>+</sup> system, Thermo Scientific (Waltham, MA, USA). The survey scans were acquired using an Al K $\alpha$  gun with a spot size of 900  $\mu\text{m}$ , a pass energy of 100.0 eV, and an energy step size of 1.00 eV. For the high-resolution XPS spectra, the pass energy was set to 10.0 eV, the energy step size was 0.10 eV, and 10 scans were accumulated.

### 3. Results and Discussion

The MAPLE-deposited films using a 266 nm irradiating wavelength are very smooth and the surface is droplet-free. The deposited films have low roughness: less than 1 nm on  $5 \times 5 \mu\text{m}^2$  for films with a thickness in the range 400–2000 nm; however, at micrometric scale, the surface has a wave-like aspect (Figure 1).

The films present a slight hydrophobic tendency, with contact angles in the range 92–105° on samples prepared by MAPLE at a 266-nm wavelength.

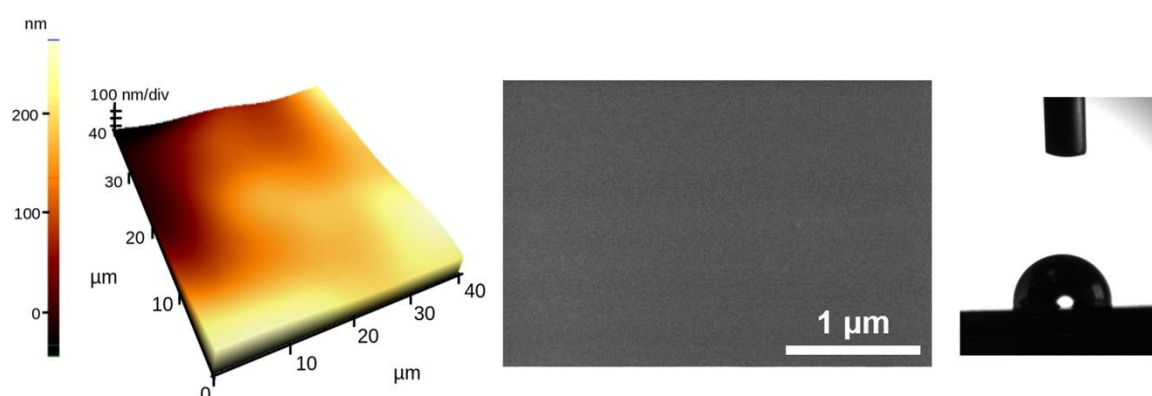


**Figure 1.** AFM and SEM images on a shellac film deposited from a 1 wt % shellac in a methanol frozen target on an Si substrate as a result of 72,000 pulses at a 266-nm wavelength with a fluence of 0.5 J/cm<sup>2</sup>. RMS roughness is 23 nm on 40  $\times$  40  $\mu\text{m}^2$ . The water contact angle is 97.2°.

Profilometric studies on the shellac films deposited using UV-irradiated light revealed deposition rates between 0.01 and 0.3  $\text{\AA}/\text{pulse}$  for using fluences in the range 0.5–2 J/cm<sup>2</sup> (Figure 2). A significant increase was obtained when using a higher amount of shellac as a guest molecule in the target. The deposition rate as a function of fluence has very interesting behavior; there is no evident increase with fluence. More than that, a decrease of the deposition rate is encountered upon increasing the laser fluence when the target contained 2 wt % shellac. It has also been reported in Ref. [25] the case of depositing lysozyme and myoglobin proteins where the deposition rate increases up to a maximum, after which it has a clear decrease. This may be due to a low sticking coefficient on the already deposited film or to the ejection of the fragmented shellac scattered from the normal direction onto the target [25]. Additionally, at high fluences and higher shellac concentrations, the amount of the evaporated solvent molecules and fragments are higher, leading to a pressure increase in the deposition chamber, which blocks shellac to reach the substrate.

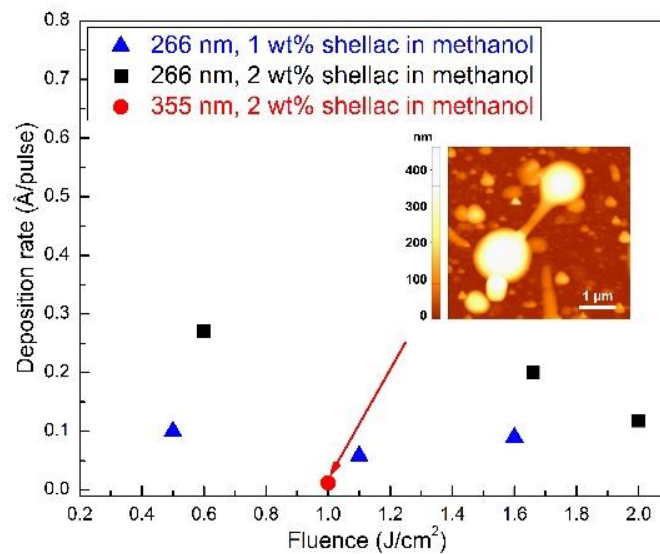


**Figure 2.** Dependence of shellac deposition rate on the laser fluence as resulting from profilometry on samples prepared by matrix-assisted pulsed laser evaporation (MAPLE). Inset AFM image on a shellac film deposited on an Si substrate using 355 nm laser wavelength as a result of 72,000 pulses at 1 J/cm<sup>2</sup> from a 2 wt % shellac in a methanol frozen target.

The very low deposition rate obtained for the experiments performed by using the 355 nm laser wavelength (the red circle on Figure 2) corroborated with the high roughness of the surface covered with droplets and elongated structures (inset Figure 2) preventing the utilization of this wavelength for shellac deposition in applications where a continuous and smooth film is needed. As already mentioned in the experimental part, the use of the 532 nm and 1064 nm irradiation wavelengths did not even lead to the deposition of continuous films. The few aggregates that could be seen on the substrate are related to the absorption of laser light by defects, seed electrons, and impurities in the frozen target, which lead to material transfer onto the substrate. Taking into consideration all these aspects, the following experiments involved the use of films deposited using the 266 nm laser wavelength.

The surface analysis revealed smooth films with low roughness grown at low fluences, unlike the case for higher fluences, where the surface is covered with wrinkle-like structures (Figure 3). Such features were previously explained upon molecular dynamics simulations of the MAPLE process [26,27]. They originate from large clusters of target material, including the solvent, which are ejected from the frozen target and deposited onto the substrate, followed in a second stage by solvent evaporation from the substrate and film formation.

As a conclusion, for experiments on the film's behavior upon immersion in SGF, the low range of fluences with values up to 0.6 J/cm<sup>2</sup> were chosen.

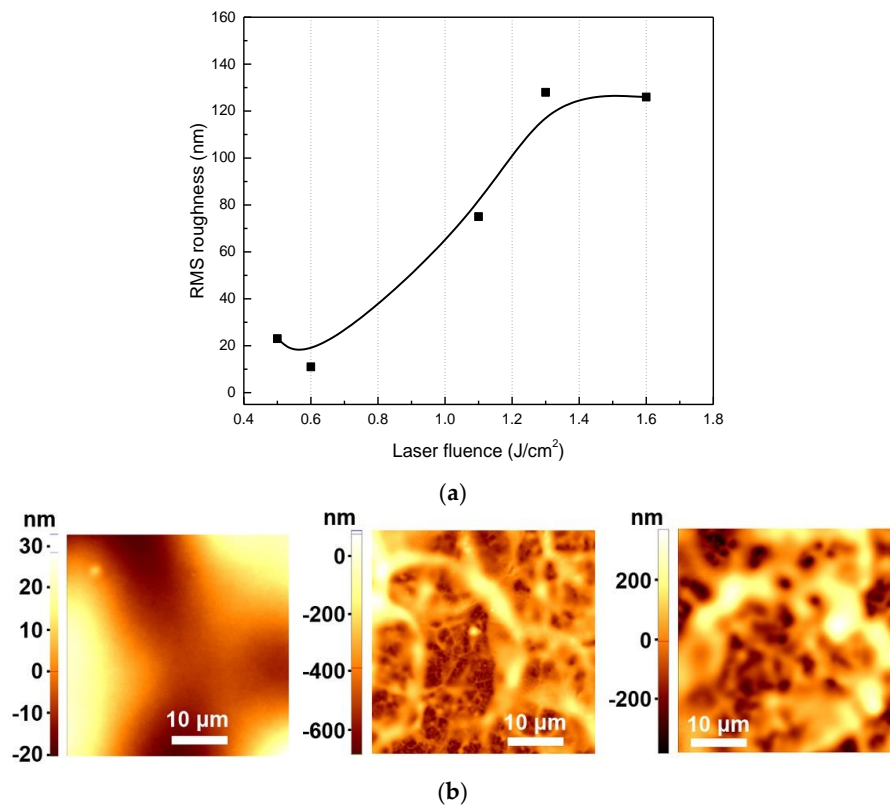


**Figure 3.** (a) The RMS roughness determined for areas of  $40 \times 40 \mu\text{m}^2$  for shellac films deposited by MAPLE. The line between the points is for eye-guidance; (b) From left to right: AFM images for 0.6, 1.3, and  $1.6 \text{ J/cm}^2$ .

Fourier transform infrared spectroscopy (FTIR) investigations were performed on films deposited by MAPLE and the results were compared to the pristine material. The laser fluence and the amount of shellac in the target solution were the investigated parameters (Figure 4).

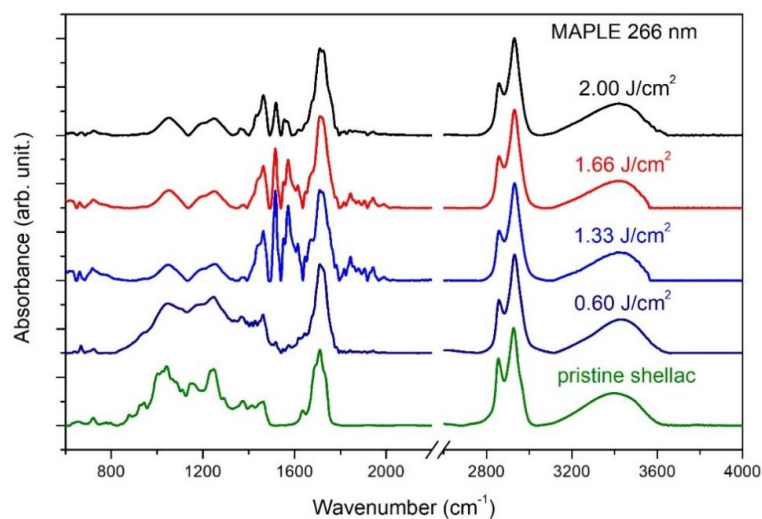


**Figure 4.** FTIR spectra of shellac films.

The large band in the range  $3100\text{--}3700 \text{ cm}^{-1}$  with a maximum at about  $3420 \text{ cm}^{-1}$  is attributed to the O–H stretching vibration, while the O–H bending vibration is identified at  $1250 \text{ cm}^{-1}$ . The strong

symmetric and asymmetric stretching vibrations of  $\text{CH}_2$  can be easily identified at  $2855\text{ cm}^{-1}$  and  $2932\text{ cm}^{-1}$ , respectively. The other two strong vibrations peaked at  $1712\text{ cm}^{-1}$  and  $1733\text{ cm}^{-1}$  are attributed to the  $\text{C}=\text{O}$  stretching vibration of esters [23] and acids, respectively [28,29]. The other medium bands of the characteristic fingerprint are:  $1636\text{ cm}^{-1}$  corresponding to the  $\text{C}=\text{C}$  stretching vibration of vinyl [30]; and  $1463\text{ cm}^{-1}$  and  $1376\text{ cm}^{-1}$  are attributed to  $\text{CH}_3$  asymmetric and symmetric bending, respectively [31]. The weak signal at  $1412\text{ cm}^{-1}$  was associated to the  $\text{CH}_2$  group attached to the ester chain as reported in Zumbühl et al. in [32]. The absorption bands at  $1175$  and  $1050\text{ cm}^{-1}$  may be due to stretching vibrations of  $\text{C}-\text{O}$  and  $\text{C}-\text{C}$  bonds [31]. Weak signals can be seen at  $944$  and  $882\text{ cm}^{-1}$  for pristine shellac, dropcast, and the low fluence used of  $0.6\text{ J/cm}^2$ . They can be attributed to the  $\text{O}-\text{H}$  out-of-plane deformation in carboxylic acids, to the  $\text{C}-\text{H}$  out-of-plane deformation in aldehydes, or to their combination [33].

The FTIR spectra show that the general aspect of the spectra of shellac deposited using laser fluences up to  $2\text{ J/cm}^2$  is not changed, leading to the conclusion that a significant part of the film material remains unaffected by the laser transfer process. The best concordance with the pristine shellac of the intensities ratio was obtained for low fluences, where all shellac characteristic absorption bands can be found. However, at laser fluences of at least  $1.33\text{ J/cm}^2$ , one can notice the appearance of two additional bands in the region  $1400\text{--}1600\text{ cm}^{-1}$ , namely at  $1515$  and  $1550\text{ cm}^{-1}$ , related to the symmetric and antisymmetric stretching modes of carboxylate moieties ( $\text{COO}^-$ ) formed upon deprotonation of the carboxylic acids of shellac [34]. This is accompanied by a decrease of  $\text{C}-\text{O}$  and  $\text{C}-\text{C}$  stretching bands at  $1175$  and  $1050\text{ cm}^{-1}$ , suggesting a tendency for material crosslinking upon laser transfer, which was confirmed by the broadening of the bands and the loosening of the fine structure noticed at large fluences.

#### 4. Acidic Solution Resistance on Samples Prepared by MAPLE Deposition

As mentioned in the experimental part, we have investigated the enteric capacity of shellac to be used as a coating for colon-targeted drugs. The chemical evolution of shellac in simulated gastric fluid (SGF) was analyzed at different time intervals. The time intervals were selected in accordance with [35]. Figure 5 presents the FTIR spectrum for a film immersed for 240 min in SGF. We have calculated and compared the intensities of the strong absorption bands from  $3423\text{ cm}^{-1}$  ( $\text{O}-\text{H}$ ) and  $1711\text{ cm}^{-1}$  ( $\text{C}=\text{O}$ ) normalized to the strongest band in the spectra appearing at  $2933\text{ cm}^{-1}$  for the films immersed in SGF to the as-deposited films.

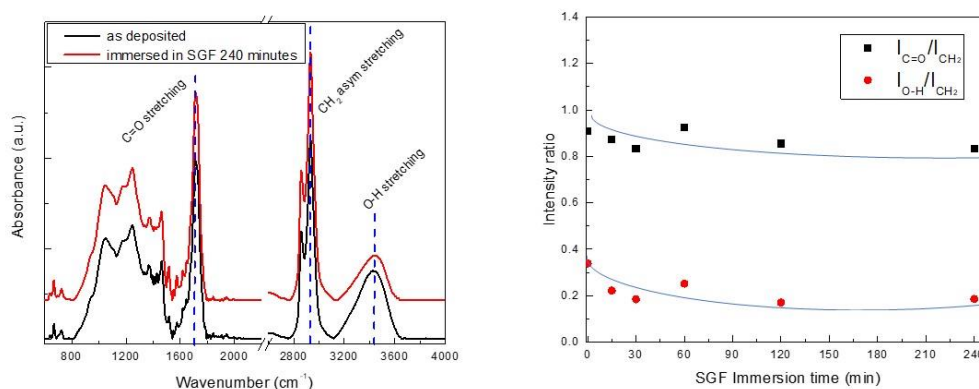


**Figure 5.** FTIR spectra of shellac film as-deposited and film immersed in simulated gastric fluid (SGF) for 240 min. Relative intensities of the absorption bands of  $\text{O}-\text{H}$  and  $\text{C}=\text{O}$  ( $3423$  and  $1711\text{ cm}^{-1}$ , respectively) normalized to the  $\text{CH}_2$  band (the strongest band of at  $2927\text{ cm}^{-1}$ ).

It is clear that no significant modification in the material composition occurs even upon immersion of the shellac film into SGF for 240 min. Upon the first 30 min of exposure to SGF, a low decrease of the populations of the  $\text{C}=\text{O}$  stretching vibration of esters and the  $\text{O}-\text{H}$  stretching vibration relative

to stretching vibrations of  $\text{CH}_2$  identified at  $2927\text{ cm}^{-1}$  was noticed. Nevertheless, upon a longer time of exposure in SGF, the shellac films were stable in the acidic gastric medium, no significant transformation could be identified, and the analyzed populations remained approximately constant up to the maximum investigated time of 240 min, which corresponds to the typical passage time through the digestive system.

The modification of surface chemical composition upon immersion in SGF, as revealed by the XPS survey spectra, is presented in Figure 6. It is shown that a slightly higher amount of oxygen is present in the MAPLE-deposited film as compared to the dropcasted shellac. Also, an incorporation of nitrogen onto the shellac surface appears and its concentration increases from 2.63% at 15 min of immersion up to 5.02% at 240 min of immersion. This is associated with pepsin interaction with shellac films, leading to the covalent attachment of nitrogen to the shellac structure.

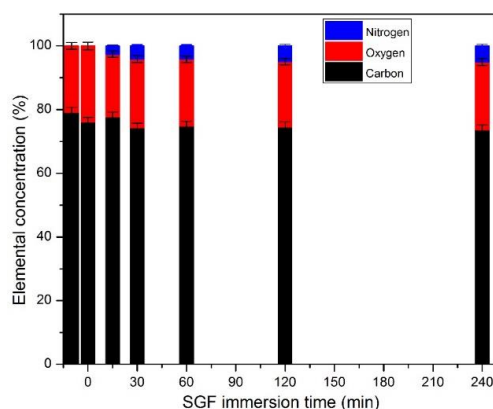


**Figure 6.** Dependence of the surface elemental concentration on the SGF immersion time.

The high-resolution XPS spectra in the carbon binding energy region were deconvoluted both for the shellac material and for those kept in SGF for various times; the results for the 240 min immersion are presented in Figure 7.

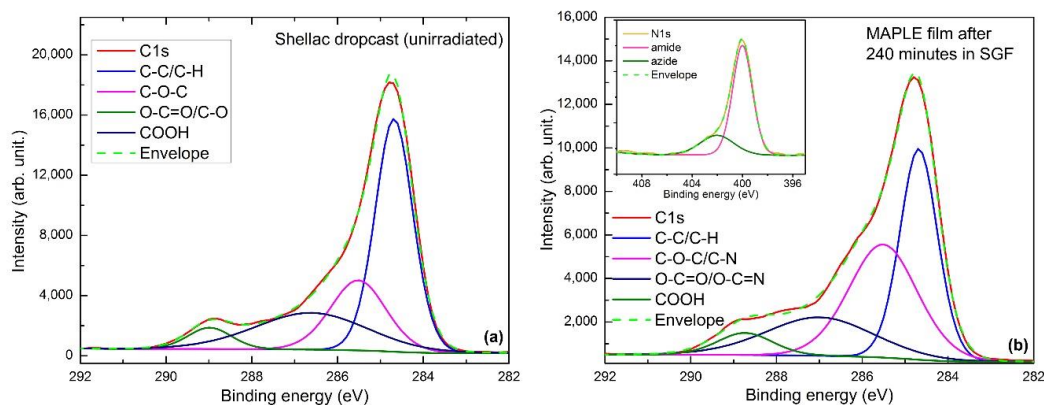


**Figure 7.** High resolution C 1s and fitting for non-irradiated shellac (a) and for a sample immersed in gastric fluid for 240 min (b).

The spectrum of the initial shellac film is dominated by the C–C/C–H peak at 284.8 eV, while larger peaks at 285.7 eV and 286.7 eV are assigned to  $\text{C–O–C}$  hydroxyl ether and  $\text{O–C=O/C*–O}$  carbonyl peaks, respectively. At higher binding energies, around 289.1 eV the presence of a COOH carboxyl peak is noticed. Upon the interaction of the shellac film with the SGF, one can see the diminution of C–C/C–H-related bonds accompanied by a significant increase and widening of the peak at 285.7 eV.

This counts as C–N bonding, which superimposes on the \*C–O–C\* from the shellac, and it appears on the film surface upon the interaction with the pepsin. Looking into the N 1s high-resolution spectra, presented in the inset of Figure 7, one can see that the main nitrogen-related bonds are those related to the amide formation, peaked at 400.0 eV, as well as those associated with the protonated nitrogen obtained upon interaction with COOH functionalities [36]. The results are consistent with the increase of nitrogen atomic concentration with the time of immersion in SGF.

The thickness of the films remained intact for all the investigated samples. The interaction of the shellac film with the SGF was evaluated also by means of AFM measurements. We performed analysis of 2000-nm-thick films with an RMS roughness of 0.7–1 nm over a scanned area of  $5 \times 5 \mu\text{m}^2$ . The step profile measurements show that the film's thickness does not modify significantly even upon 240 min immersion. Nevertheless, the roughness increases by 1 order of magnitude even for an immersion time as low as 15 min and reaches 12.3 nm upon 120 min of immersion. Small pores, both regarding their diameter and depth, had appeared on the shellac surface already upon 15 min of immersion (Figure 8). The pores' density and their depth increases when the exposure time to SGF increases; however, the largest pore identified after 4 h of immersion had a depth of 85 nm, which represents less than 5% of the film's thickness.

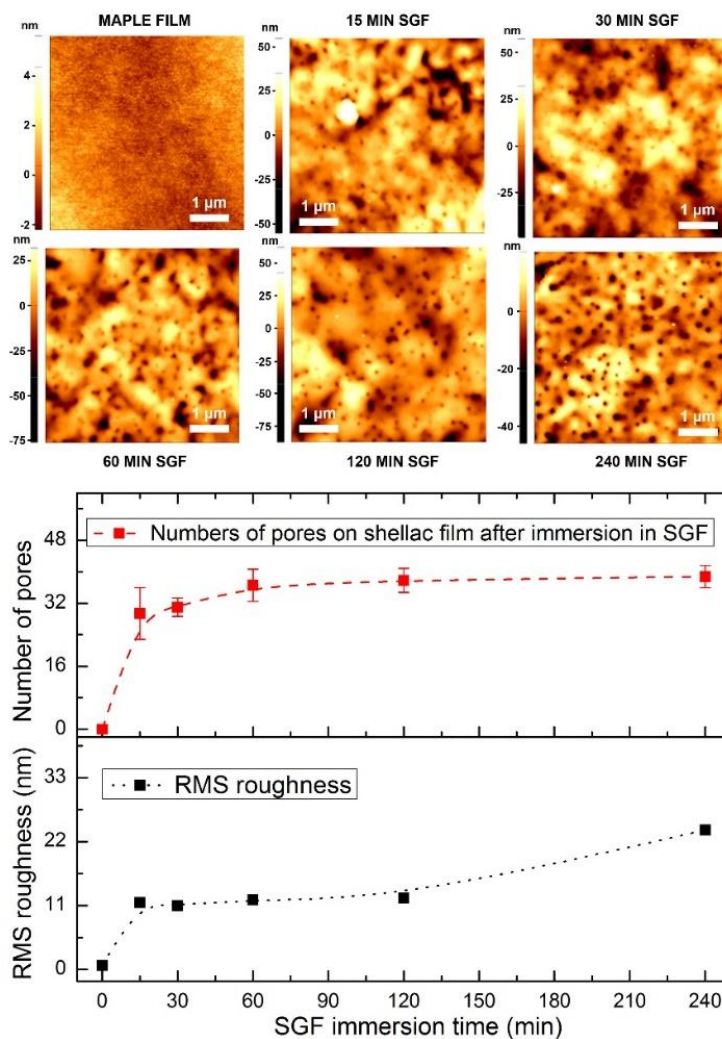


**Figure 8.** AFM images on  $5 \times 5 \mu\text{m}^2$  films of MAPLE shellac films immersed in SGF for different time durations. RMS Roughness on  $5 \times 5 \mu\text{m}^2$  and number of pores counted on  $5 \mu\text{m}^2$ . The MAPLE films have a thickness of 2000 nm and were deposited using 2% shellac dissolved in methanol with a fluence of  $0.6 \text{ J}/\text{cm}^2$  and 72,000 pulses.

The behavior of MAPLE-deposited shellac films upon immersion in SGF for 240 min was compared to that of films deposited by the dropcast method and submitted to the same environment. The AFM images are presented in Figure 9. The  $5 \times 5 \mu\text{m}^2$  AFM image for the dropcast film, before SGF immersion, presents a smooth film, with an RMS roughness of 0.6 nm. After SGF immersion, the surface of the film is strongly changed; the film is very rough and holes similar to those noticed in the case of MAPLE films can be identified. Nevertheless, the higher roughness of the dropcast films after immersion (88 nm measured on  $5 \times 5 \mu\text{m}^2$ ) compared to the MAPLE films also supports the hypothesis that the MAPLE technique produces more dense and compact films. This can be associated with the higher impinging energy of the material reaching the substrate in the case of MAPLE processing, which leads to a more compact deposit with respect to the softer dropcast process.

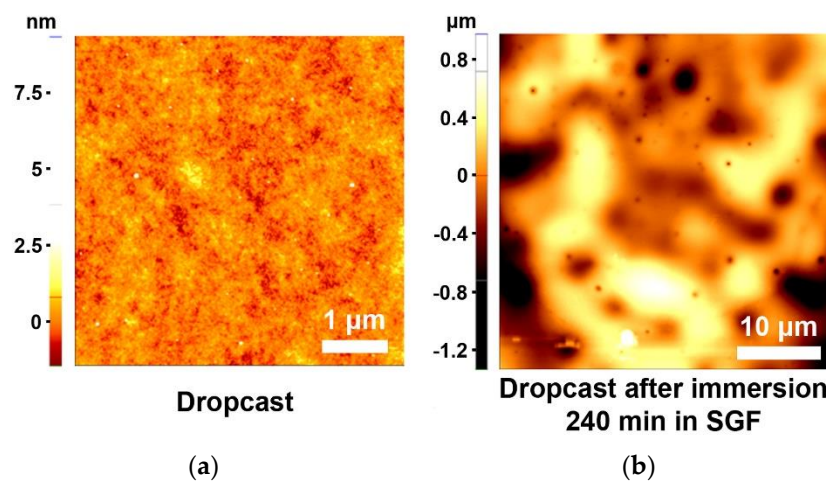


**Figure 9.** AFM image on  $5 \times 5 \mu\text{m}^2$  on a dropcast film (a); AFM image on  $40 \times 40 \mu\text{m}^2$  after 240 min immersion in SGF (b).

## 5. Conclusions and Outlook

The deposition of shellac thin films by MAPLE has proven to be successful by utilization of a UV laser. The obtained samples have low roughness and are droplet-free. We have obtained films with a thickness of 2000 nm and an RMS roughness less than 1% of the thickness for the optimal set of deposition parameters. It can be seen that laser fluence is an important factor in preserving the chemical structure of shellac. For low fluences, all the characteristic absorption bands were found and the best concordance to the pristine shellac was obtained. Upon immersion in Simulated Gastric Fluid, the thickness of the films remained intact even upon 240 min of immersion. The surface of the films changed even for an immersion time as low as 15 min, and the roughness increased as a result of the appearance of holes. The pores' density and size increased when the exposure time to SGF increased, but the biggest hole measured after 240 min in SGF had a depth of just 85 nm. This behavior, corroborated with the UV resistance [28] we have demonstrated previously, makes MAPLE shellac films promising for use as an enteric coating and opens the path for a variety of applications.

**Author Contributions:** Investigation, S.B.; Formal Analysis, A.B. and V.M.; Conceptualization, A.M.; Supervision, B.M.; Writing—Review & Editing, A.M., B.M., S.B., A.B. and V.M.

**Funding:** This research was funded by the Romanian National Authority for Scientific Research and Innovation, CNCS—UEFISCDI (PN-III-P2-2.1-PED-2016-0221 (contract PED 94/2017)—“IPOD”).

**Conflicts of Interest:** The authors declare no conflict of interest.

## References

1. Yates, P.; Field, G.F. Shellolic acid, a cedrenoid sesquiterpene from shellac. *J. Am. Chem. Soc.* **1960**, *82*, 5764–5765. [CrossRef]
2. Colombini, M.P.; Bonaduce, I.; Gautier, G. Molecular pattern recognition of fresh and aged shellac. *Chromatographia* **2003**, *58*, 357–364.
3. Irimia-Vladu, M.; Głowacki, E.D.; Schwabegger, G.; Leonat, L.; Zekiye Akpınar, H.; Sitter, H.; Bauer, S.; Sariciftci, N.S. Natural resin shellac as a substrate and a dielectric layer for organic field-effect transistors. *Green Chem.* **2013**, *15*, 1473–1476. [CrossRef]
4. Palou, L.; Valencia-Chamorro, S.A.; Pérez-Gago, M.B. Antifungal edible coatings for fresh citrus fruit: A review. *Coatings* **2015**, *5*, 962–986. [CrossRef]
5. Hult, E.L.; Iotti, M.; Lenes, M. Efficient approach to high barrier packaging using microfibrillar cellulose and shellac. *Cellulose* **2010**, *17*, 575–586. [CrossRef]
6. Loy, M.; Riddell, L. The effect of shellac nail polish on measurement of oxygen saturation by pulse oximetry. *Anaesthesia* **2014**, *69* (Suppl. S3), 42.
7. Sutherland, K.; del Río, J.C. Characterization and discrimination of various types of lac resin using gas chromatography mass spectrometry techniques with quaternary ammonium reagents. *J. Chromatogr. A* **2014**, *1338*, 149–163. [CrossRef] [PubMed]
8. Singhababu, Y.N.; Choudhary, S.K.; Shukla, N.; Das, S.; Sahu, R.K. Observation of large positive magneto-resistance in bubble decorated graphene oxide films derived from shellac biopolymer: A new carbon source and facile method for morphology-controlled properties. *Nanoscale* **2015**, *7*, 6510–6519. [CrossRef] [PubMed]
9. Weththimuni, M.L.; Capsoni, D.; Malagodi, M.; Milanese, C.; Licchelli, M. Shellac/nanoparticles dispersions as protective materials for wood. *Appl. Phys. A* **2016**, *122*, 1058. [CrossRef]
10. Lausecker, R.; Badilita, V.; Gleißner, U.; Wallrabe, U. Introducing natural thermoplastic shellac to microfluidics: A green fabrication method for point-of-care devices. *Biomicrofluidics* **2016**, *10*, 044101. [CrossRef] [PubMed]
11. Campbell, A.L.; Stoyanov, S.D.; Paunov, V.N. Novel multifunctional micro-ampoules for structuring and encapsulation. *Chem. Phys. Chem.* **2009**, *10*, 2599–2602. [CrossRef] [PubMed]
12. Sinha, V.R.; Kumira, R. Coating polymers for colon specific drug delivery: A comparative in vitro evaluation. *Acta Pharm.* **2003**, *53*, 41–47. [PubMed]
13. Farag, Y.; Leopold, C.S. Development of shellac-coated sustained release pellet formulations. *Eur. J. Pharm. Sci.* **2011**, *42*, 400–405. [CrossRef] [PubMed]
14. Schad, B.; Smith, H.; Cheng, B.; Scholten, J.; VanNess, E.; Riley, T. Coating and taste masking with shellac. *Pharm. Technol.* **2013**, *2013* (Suppl. S5). Available online: <http://www.pharmtech.com/coating-and-taste-masking-shellac?pageID=2> (accessed on 14 June 2018).
15. Kumpugdee-Vollrath, M.; Tabatabaeifar, M.; Helms, M. New coating materials based on mixtures of shellac and pectin for pharmaceutical products. *Int. Sch. Sci. Res. Innov.* **2014**, *8*, 21–29.
16. Wang, X.; Yu, D.-G.; Li, X.-Y.; Bligh, S.W.A.; Williams, G.R. Electrospun medicated shellac nanofibers for colon-targeted drug delivery. *Int. J. Pharm.* **2015**, *490*, 384–390. [CrossRef] [PubMed]
17. Somacescu, S.; Scurtu, R.; Epurescu, G.; Pascu, R.; Mitu, B.; Osiceanu, P.; Dinescu, M. Thin films of SnO<sub>2</sub>-CeO<sub>2</sub> binary oxides obtained by pulsed laser deposition for sensing application. *Appl. Surf. Sci.* **2013**, *278*, 146–152. [CrossRef]
18. Schöning, M.J.; Mourzina, Y.G.; Schubert, J.; Zander, W.; Legin, A.; Vlasov, Y.G.; Lüth, H. Pulsed laser deposition—An innovative technique for preparing inorganic thin films. *Electroanalysis* **2001**, *13*, 727–732. [CrossRef]
19. Brodoceanu, D.; Scarisoreanu, N.D.; Filipescu, M.M.; Epurescu, G.N.; Matei, D.G.; Verardi, P.; Craciun, F.; Dinescu, M. Pulsed laser deposition of oxide thin films. In *Plasma Production by Laser Ablation*; Gammino, S., Mezzasalma, A.M., Neri, F., Torrisi, L., Eds.; World Scientific Publishing Co. Pte. Ltd.: Singapore, 2004; pp. 41–46, ISBN 9789812702555.
20. Houser, E.J.; Chrisey, D.B.; Bercu, M.; Scarisoreanu, N.D.; Purice, A.; Colceag, D.; Constantinescu, C.; Moldovan, A.; Dinescu, M. Functionalized polysiloxane thin films deposited by matrix-assisted pulsed laser evaporation for advanced chemical sensor applications. *Appl. Surf. Sci.* **2006**, *252*, 4871–4876. [CrossRef]

21. Purice, A.; Schou, J.; Kingshott, P.; Dinescu, M. Production of active lysozyme films by matrix assisted pulsed laser evaporation at 355 nm. *Chem. Phys. Lett.* **2007**, *435*, 350–353. [[CrossRef](#)]
22. Birjega, R.; Matei, A.; Mitu, B.; Ionita, M.D.; Filipescu, M.; Stokker-Cheregi, F.; Luculescu, C.; Dinescu, M.; Zavoianu, R.; Pavel, O.D.; et al. Layered double hydroxides/polymer thin films grown by matrix assisted pulsed laser evaporation. *Thin Solid Films* **2013**, *543*, 63–68. [[CrossRef](#)]
23. Ravi, V.; Pramod Kumar, T.M.; Siddaramaiah. Novel colon targeted drug delivery system using natural polymers. *Indian J. Pharm. Sci.* **2008**, *70*, 111–113. [[PubMed](#)]
24. Warren, C.R. Rapid measurement of chlorophylls with a microplate reader. *J. Plant Nutr.* **2008**, *31*, 1321–1332. [[CrossRef](#)]
25. Matei, A.; Schou, J.; Constantinescu, C.; Kingshott, P.; Dinescu, M. Growth of thin films of low molecular weight proteins by matrix assisted pulsed laser evaporation (MAPLE). *Appl. Phys. A* **2011**, *105*, 629–633. [[CrossRef](#)]
26. Sellinger, A.; Leveugle, E.; Fitz-Gerald, J.-M.; Zhigilei, L.V. Generation of surface features in films deposited by matrix-assisted pulsed laser evaporation: The effects of the stress confinement and droplet landing velocity. *Appl. Phys. A* **2008**, *92*, 821–829. [[CrossRef](#)]
27. Leveugle, E.; Zhigilei, L.V. Molecular dynamics simulation study of the ejection and transport of polymer molecules in matrix-assisted pulsed laser evaporation. *J. Appl. Phys.* **2007**, *102*, 074914. [[CrossRef](#)]
28. Bercea, A.; Mitu, B.; Matei, A.; Marascu, V.; Brajnicov, S. Esterification process induced by UV irradiation of shellac thin films deposited by matrix assisted pulsed laser evaporation. Unpublished work, 2018.
29. Derrick, M.; Stulik, D.; Landry, J.M. *Infrared Spectroscopy in Conservation Science. Scientific Tools for Conservation*; Ball, T., Tidwell, S., Eds.; Getty Publications: Los Angeles, CA, USA, 1999.
30. Derrick, M. Fourier transform infrared spectral analysis of natural resins used in furniture finishes. *JAIC* **1989**, *28*, 43–56.
31. Licchelli, M.; Malagodi, M.; Somaini, M.; Weththimuni, M.; Zanchi, C. Surface treatments of wood by chemically modified shellac. *Surf. Eng.* **2013**, *29*, 121–127. [[CrossRef](#)]
32. Zumbühl, S.; Hochuli, A.; Soulier, B.; Scherrer, N.C. Fluorination technique to identify the type of resin in aged vanishes and lacquers using infrared spectroscopy. *Microchem. J.* **2017**, *134*, 317–326. [[CrossRef](#)]
33. Shearer, G.L. An Evaluation of Fourier Transform Infrared Spectroscopy for the Characterization of Organic Compounds in Art and Archaeology. Ph.D. Thesis, University College London, London, UK, October 1989.
34. Oomens, J.; Steill, J.D. Free carboxylate stretching modes. *J. Phys. Chem. A Lett.* **2008**, *112*, 3281–3283. [[CrossRef](#)] [[PubMed](#)]
35. Camilleri, M.; Colemont, L.J.; Phillips, S.F.; Brown, M.L.; Thomforde, G.M.; Chapman, N.; Zinsmeister, A.R. Human gastric emptying and colonic filling of solids characterized by a new method. *Am. J. Physiol.* **1989**, *257*, 84–90. [[CrossRef](#)] [[PubMed](#)]
36. Alzate-Carvajal, N.; Basiuk, E.V.; Meza-Laguna, V.; Puente-Lee, I.; Farías, M.H.; Bogdanchikova, N.; Basiuk, V.A. Solvent-free one-step covalent functionalization of graphene oxide and nanodiamond with amines. *RSC Adv.* **2016**, *6*, 113596. [[CrossRef](#)]

